Proceedings of the 30th International Cosmic Ray Conference
Rogelio Caballero, Juan Carlos D'Olivo, Gustavo Medina-Tanco,
Lukas Nellen, Federico A. Sánchez, José F. Valdés-Galicia (eds.)
Universidad Nacional Autónoma de México,
Mexico City, Mexico, 2008

Vol. 2 (OG part 1), pages 501–504

30TH INTERNATIONAL COSMIC RAY CONFERENCE

A Revised Catalogue of EGRET Sources

JEAN-MARC CASANDJIAN[1], ISABELLE GRENIER[1]
[1]*AIM, Service d'Astrophysique, CEA Saclay, 91191 Gif/Yvette, France*
casandjian@cea.fr

Abstract: We have searched for γ-ray sources in the EGRET data from cycles 1 to 9, using a binned maximum-likelihood method and detection thresholds similar to those used for the 3rd EGRET catalogue. Two interstellar background models were developed based on different assumptions for the cosmic-ray distribution in the Galaxy: the GALPROP diffusion model and a radial gradient of the γ-ray emissivity per atom as fitted to the EGRET data. Both models used new gas maps from recent HI and CO surveys, as well as an additional dark gas component associated with cold dust in the local clouds. The resulting source list strongly differs from the 3EG catalogue, one third of the sources having changed either in position or in flux and significance. These changes primarily affect the unidentified sources that are largely explained by the new gas data and by the dark gas envelopes of the Gould Belt clouds.

Introduction

The Energetic Gamma-Ray Experiment Telescope (EGRET), which operated on Compton-GRO from April 1991 to May 2000, detected photons in the 20 MeV to 30 GeV range. The official EGRET catalogue (hereafter 3EG) was published by Hartman et al. [1] and listed 271 point sources shining above 100 MeV, including a solar flare, the Large Magellanic Cloud, five pulsars, one radio galaxy, and 66 high-confidence identifications of blazars. In addition, 27 lower confidence blazar identifications were given. In 1999, 3EG contained 170 unidentified sources with no known counterpart at lower energy. About 150 of them are still unidentified. Their origin is an intriguing and long lasting question. Candidate counterparts include pulsar wind nebulae, supernova remnants, blazars and nearby radiogalaxies, X-ray binaries, microquasars, gas clouds, massive stars, nearby starburst galaxies, and galaxy clusters. It was also noticed [2,3] that the steadiest and faintest unidentified sources at mid latitudes are significantly correlated with the Gould Belt, a nearby structure of massive stars and large clouds surrounding the Sun.
These sources are detected above the intense background of interstellar radiation due to cosmic-ray (CR) interactions in the Milky Way. In order to extract a point-source significance, position, and flux, this diffuse emission has to be carefully modelled, both in flux and in its complex structure. We have revised this model taking advantage of recent cloud and interstellar radiation field data and we present a new catalogue of EGRET sources found above 100 MeV in the full 9 years of EGRET data.

The Galactic Diffuse Emission

The interstellar emission is produced by the interaction of energetic cosmic-ray electrons and protons with the interstellar gas and soft radiation. The decay of π^0 produced in pp-collisions accounts for most of the γ rays at energy between 100 MeV and 10 GeV. Inverse Compton (IC) scattering of the interstellar radiation field by electrons and positrons and Bremsstrahlung emission are the other main contributors to the diffuse γ rays. For the purpose of this analysis, we have derived a new model based on the realistic hypothesis that, if energetic cosmic rays uniformly penetrate all interstellar gas phases, the γ-ray intensity in each direction can be modelled as a linear combination of gas column-densities plus the Galactic inverse Compton intensity (I_{IC}), and

an isotropic extragalactic background intensity (I_E).

The census of atomic and molecular gas in the Milky Way mainly comes from the radio HI and CO line surveys. To allow for gradients of the CR density along the lines of sight, the radial velocity information in the HI and CO line data and a model for the rotation of the Galaxy has been used to partition the gas by Galactocentric distance into rings of 2 to 4 kpc width (Digel et al. 2007, in preparation). We have used the new all-sky Leiden-Argentina-Bonn composite HI survey [4] to derive N_{HI} column-densities and the velocity-integrated CO brightness temperature map, W_{CO}, from the CfA compilation at $|b| \leq 32°$ [5]. W_{CO} empirically scales to $N(H_2)$ column-density via the $X = N(H_2)/W_{CO}$ ratio. The regions outside the CO survey boundaries should be mostly free of bright CO emission.

For the first time, we have included in the interstellar model the large column-densities N_{dark} of "dark" gas associated with cold dust at the transition between the atomic and molecular phases [6]. This transitional phase where HI turns into H_2 is not seen in radio, but is revealed by the γ-ray emission from cosmic rays flooding it and by its dust content (very cold thermal emission and anomalous dust emission near 20 GHz). The column-densities, clumpiness, and large spread across the sky of the dark-gas envelopes of the nearby clouds in the Gould Belt and the Galactic plane can strongly affect source detectability.

The CR density falls with radial (Galactocentric) distance [7]. To account for the resulting emissivity gradient, we model γ-ray counts in a given direction as: $N_\gamma(l,b) = \varepsilon(l,b) \times [\sum_{ring} q_{HI}.N_{HI}(l,b) + \sum_{ring} q_{CO}.W_{CO}(l,b) + q_{dark}.N_{dark}(l,b) + q_{IC}.I_{IC}(l,b) + I_{ex}]$ where we sum up contributions from rings of different emissivities (q) along the line of sight. The input maps were convolved with the EGRET PSF for an input $E^{-2.1}$ spectrum. ε(l,b) notes the EGRET exposure map. The inverse Compton map was calculated by GALPROP 6002029RB [8]. The q emissivities in each ring were fitted to the γ-ray data by means of a maximum-likelihood test with Poisson statistics in three energy bands (>100MeV, 0.3-1GeV, and >1GeV).

In addition to this "ring" model of the interstellar background and in order to evaluate the impact of our poor knowledge of the cosmic-ray distribution on source detection, we have searched for sources above a second interstellar model based on the diffuse emission components calculated by GALPROP (run number 49_6002029RB, [9]) complemented with the local dark gas map. The inverse Compton, pion, bremsstrahlung, and dark-gas contributions were fitted to the EGRET data. In the rest of the text we will refer to this model as "GALPROP" even though it includes the dark gas. Given its larger flexibility, the ring model was found to best fit the EGRET data.

When searching for sources with either model, the total background map was adjusted to the data in the region of interest using the familiar *Gmult* (galactic multiplier) and *Gbias* (isotropic flux) parameters [10].

Source detection

As for 3EG, we have used a 2D binned Poisson likelihood method and the EGRET LIKE code (version 5.61) to fit the background model and to estimate the location, significance, and flux of the sources [10,1]. LIKE computes a Test Statistic (TS) value that compares the likelihood of detecting a source to the null likelihood - no source - at a given position.

The EGRET count and exposure maps come from the CGRO Science Support Center. Having been reprocessed in 2001, they differ from the datasets used for 3EG. We have used summed all-sky maps corresponding to cycles 1, 2, 3, 4, 1+2, 2+3, 1+2+3+4, 5+6, 7+8+9, and to the full 9 years of data. In addition, we have analyzed 46 individual periods for which flaring 3EG sources had been detected. As for the summed maps, the individual period maps retain only photons within 30° from the instrument axis. Photons and exposure maps were binned to 0.5^ox0.5^o.

For the 3EG catalogue, sources were detected in the integrated E > 100 MeV band. TS-maps were then constructed in 3 energy bands (>100MeV, 0.3-1GeV, and >1GeV) from the observation with highest TS and a source final position was obtained from the smallest error contours. Given the modern computer performance, we have directly searched for sources independently in the three energy bands.

We have divided each of the 10 all-sky cycle maps in 45 zones, both in Galactic and equatorial

coordinates, with a large overlap. The use of both coordinate systems is required to account for source deformation in rectangular projection at high latitude or declination. For each zone, each individual period, and each of the 3 energy bands, we calculated a TS map for excesses above the background. Sources were iteratively detected from high TS to low TS in successive TS-maps. Between each steps, the detected sources were included in the background model until no excess with $\sqrt{TS} > 3$ was left in the final TS-map. The TS-map peak positions were automatically measured and converted into source position by taking the center of the 95% confidence ellipse contour around this position. Source positions were calculated at each iteration to take into account the influence of the neighbouring sources. More than 1100 TS-maps were calculated at the CCIN2P3 Computing Center's resources.

Most sources were thus given 2 positions per energy band and observation, one from the Galactic coordinate map and one from the equatorial one. We cross-compared the two and selected the position from the least deformed projection. Sources with only one position were not included in the list unless their latitude or declination were higher than 40° or their longitude or right-ascension were close to the map edges.

At this stage, sources have 3 positions with energy for a given observation. We chose among the three the position corresponding to the smallest 95% confidence contour, unless its $TS^{1/2}$ in another band was more than 1.5 higher. This condition reduces the risk of incorrect source assignment during the cross-comparison phase. Sources found at low energy, but not at high energy were included in the list, as well as sources found only at high energy.

We then used the same criteria to cross-compare individual periods and summed cycles in order to obtain a final list of candidate sources with the best position from the different energy bands and periods/cycles. Their fluxes above 100 MeV were finally calculated at this position for the different periods and cycles.

We followed this procedure with both the ring and GALPROP interstellar backgrounds. Sources that did not meet the EGRET detection threshold ($\sqrt{TS} > 5$ at $|b| < 10°$ and $\sqrt{TS} > 4$ elsewhere) with the ring model and $\sqrt{TS} > 3$ with the GALPROP model were considered too model dependent and were excluded from the catalogue. Sources very close to the brightest sources (as the 3EG likely artefacts around Vela) or with low count statistics and very asymmetric 95% error contours were removed as unlikely point-source detections due to incorrect PSF tails from intense sources or to extended features not properly modelled in the Galactic emission.

Revised Catalogue

Our EGRET revised catalogue (EGR) contains 176 significant sources. Many 3EG sources have not been confirmed because of the additional Galactic emission present in the background from new HI, CO, and dark gas structures. It is interesting to note that the vast majority of unconfirmed 3EG sources (see Table 1) were unidentified, in particular those spatially correlated with the Gould Belt. Only eight 3EG sources firmly identified as AGN are not present in the new list. We do detect excesses toward them, but their significance falls below the detection threshold. It is important to note that detectability near the threshold is very sensitive to all the procedure. 151 EGR sources have a 3EG counterpart and we find a reasonable agreement in position and flux from both analyses. On the other hand, 25 EGR sources are "new" in the sense that they have no 3EG counterpart (Table 2).

Table 1: 120 3EG sources not found in EGR

0130-1758	0622-1139	1300-4406	1709-0828	1856+0114
0229+6151	0628+1847	1308+8744	1714-3857	1858-2137
0245+1758	0634+0521	1308-6112	1717-2737	1903+0550
0323+5122	0702-6212	1316-5244	1718-3313	1904-1124
0348+3510	0706-3837	1323+2200	1720-7820	1928+1733
0404+0700	0747-3412	1329+1708	1733+6017	1935-4022
0407+1710	0808-5344	1329-4602	1735-1500	1958+2909
0416+3650	0821-5814	1410-6147	1741-2050	1958-4443
0426+1333	0824-4610	1447-3936	1741-2312	2016+3657
0435+6137	0827-4247	1500-3509	1744-0310	2020-1545
0439+1555	0828-4954	1527-2358	1744-3011	2022+4317
0439+1105	0841-4356	1600-0351	1744-3934	2027+3429
0458-4635	0848-4429	1616-2221	1746-2851	2034-3110
0459+0544	0859-4257	1627-2419	1757-0711	2035+4441
0459+3352	0910+6556	1631-1018	1800-0146	2100+6012
0500+2529	1014-5705	1631-4033	1806-5005	2206+6602
0510+5545	1027-5817	1633-3216	1810-1032	2219-7941
0520+2556	1045-7630	1634-1434	1823-1314	2248+1745
0521+2147	1052+5718	1635-1751	1824+3441	2255+1943
0533+4751	1212+2304	1639-4702	1824-1514	2359+2041
0542+2610	1222+2315	1646-0704	1828+0142	
0542-0655	1227+4302	1649-1611	1834-2803	
0546+3948	1230-0247	1653-2133	1836-4933	
0556+0409	1235+0233	1659-6251	1850+5903	
0616-0720	1249-8330	1704-4732	1850-2652	

Table 2: 25 EGR sources not found in 3EG

Name	ra	dec
EGRJ0028+04	7.059	4.95
EGRJ0057-78	14.46	-78.65
EGRJ0100+49	15.01	49.45
EGRJ0141+17	25.47	17.32
EGRJ0243-59	40.94	-59.50
EGRJ0413-37	63.40	-37.69
EGRJ0509+05	77.41	5.84
EGRJ0540+06	85.06	6.95
EGR1122-59	170.55	-59.77
EGRJ1158-19	179.67	-19.83
EGRJ1259-22	194.92	-22.16
EGRJ1619+22	244.75	22.39
EGRJ1651+40	252.90	40.72
EGRJ1740+49	265.09	49.77
EGRJ1747-30	266.96	-30.76
EGRJ1757-29	269.35	-29.01
EGRJ1856+02	284.23	2.59
EGRJ1920+46	290.17	46.42
EGRJ1932-39	293.06	-39.77
EGRJ1959+43	299.78	43.38
EGRJ2027-42	306.79	-42.12
EGRJ2202+33	330.63	33.68
EGRJ2233-48	338.46	-48.21
EGRJ2258-27	344.53	-27.75
EGRJ2308+36	347.23	36.76

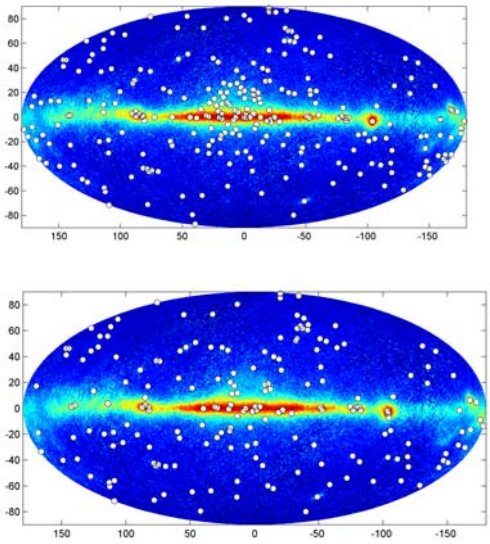

Figure 1: 3EG catalog (above) and EGR catalog (below).

Conclusion

We have searched for point-like sources in the reprocessed EGRET data from cycle 1 to 9 using new interstellar background models based on the most recent HI, CO, and dark gas data, as well as two different assumptions for the cosmic-ray distribution (the GALPROP diffusion model or a radial emissivity gradient fitted to the diffuse EGRET data). We have used the 3EG tools, likelihood method, procedure and significance threshold to detect sources, but have expanded the search to 3 different energy bands (above 100 MeV, 0.3-1 GeV, and above 1 GeV). The resulting number of detected sources has decreased by more than a third. Many unidentified sources, in particular among those spatially associated with the Gould Belt, are not confirmed as significant excesses. Their emission can be explained by the additional interstellar emission and its structure. On the other hand, 25 new possible γ-ray sources are found. Beyond this brief summary, the full publication will list the source properties and their response to the choice of cosmic-ray distributions.

References

[1] Hartman R. C., et al., 1999, ApJS 123, 79
[2] Grenier I. A., 2000, A&A 364, 93
[3] Gehrels N., et al., 2000, Nature 404, 363
[4] Kalberla P. M. W., et al., 2005, A&A 440, 775
[5] Dame T. M., et al., 2001, ApJ 547, 792
[6] Grenier I. A., et al., 2005, Science 307, 1292
[7] Strong A.W., Mattox J.R.,1996, A&A 308, 21
[8] Moskalenko I. V., et al., 2006, ApJ, 640, 155
[9] Strong A. W., et al., 2004,ApJ, 613, 962
[10] Mattox J. R., et al., 1996, ApJ, 461, 396